Received: 26 November 2020 | Revised: 4 March 2021 | Accepted: 25 March 2021

DOI: 10.1002/hbm.25434

RESEARCH ARTICLE

WILEY

Individual-based morphological brain network organization and its association with autistic symptoms in young children with autism spectrum disorder

Changchun He[1,2] | Jesus M. Cortes[3,4,5] | Xiaodong Kang[6] | Jing Cao[6] | Heng Chen[7] | Xiaonan Guo[8,9] | Ruishi Wang[1,2] | Lingyin Kong[10] | Xinyue Huang[1,2] | Jinming Xiao[1,2] | Xiaolong Shan[1,2] | Rui Feng[1,2] | Huafu Chen[1,2] | Xujun Duan[1,2]

[1]The Clinical Hospital of Chengdu Brain Science Institute, School of Life Science and Technology, University of Electronic Science and Technology of China, Chengdu, China

[2]MOE Key Lab for Neuroinformation, High-Field Magnetic Resonance Brain Imaging Key Laboratory of Sichuan Province, University of Electronic Science and Technology of China, Chengdu, China

[3]Computational Neuroimaging Laboratory, Biocruces-Bizkaia Health Research Institute, Barakaldo, Spain

[4]Ikerbasque: The Basque Foundation for Science, Bilbao, Spain

[5]Department of Cell Biology and Histology, University of the Basque Country, Leioa, Spain

[6]Affiliated Sichuan Provincial Rehabilitation Hospital of Chengdu University of TCM, Sichuan Bayi Rehabilitation Center, Chengdu, China

[7]School of Medicine, Medical College of Guizhou University, Guiyang, China

[8]School of Information Science and Engineering, Yanshan University, Qinhuangdao, China

[9]Hebei Key Laboratory of information transmission and signal processing, Yanshan University, Qinhuangdao, China

[10]Department of Biomedical Engineering, School of Material Science and Engineering, South China University of Technology, Guangzhou, China

Correspondence
Xujun Duan, The Clinical Hospital of Chengdu Brain Science Institute, School of Life Science and Technology, University of Electronic Science and Technology of China, Chengdu, China.
Email: duanxujun@uestc.edu.cn

Funding information
China Postdoctoral Science Foundation, Grant/Award Number: 2019M660236; National Natural Science Foundation of China, Grant/Award Numbers: 61901129, 62036003, 81871432, U1808204; The Basque Foundation for Science and from Ministerio de Economia, Industria y Competitividad (Spain) and FEDER, Grant/Award Number: DPI2016-79874-R; the Fundamental Research Funds for the Central Universities, Grant/Award Numbers: 2672018ZYGX2018J079, ZYGX2019Z017; the Sichuan Science and Technology Program, Grant/Award Number: 2019YJ0180

Abstract

Individual-based morphological brain networks built from T1-weighted magnetic resonance imaging (MRI) reflect synchronous maturation intensities between anatomical regions at the individual level. Autism spectrum disorder (ASD) is a socio-cognitive and neurodevelopmental disorder with high neuroanatomical heterogeneity, but the specific patterns of morphological networks in ASD remain largely unexplored at the individual level. In this study, individual-based morphological networks were constructed by using high-resolution structural MRI data from 40 young children with ASD (age range: 2–8 years) and 38 age-, gender-, and handedness-matched typically developing children (TDC). Measurements were recorded as threefold. Results showed that compared with TDC, young children with ASD exhibited lower values of small-worldness (i.e., σ) of individual-level morphological brain networks, increased morphological connectivity in cortico-striatum-thalamic-cortical (CSTC) circuitry, and decreased morphological connectivity in the cortico-cortical network. In addition, morphological connectivity abnormalities can predict the severity of social

communication deficits in young children with ASD, thus confirming an associational impact at the behavioral level. These findings suggest that the morphological brain network in the autistic developmental brain is inefficient in segregating and distributing information. The results also highlight the crucial role of abnormal morphological connectivity patterns in the socio-cognitive deficits of ASD and support the possible use of the aberrant developmental patterns of morphological brain networks in revealing new clinically-relevant biomarkers for ASD.

KEYWORDS
autism spectrum disorder, individual-based morphological brain network, small-worldness, social communication deficits, structural magnetic resonance imaging

1 | INTRODUCTION

Morphological brain networks (MBNs) characterize interregional similarities in several morphological aspects of gray matter and have recently attracted attention in the investigation of brain abnormalities in neurological diseases (Bassett et al., 2008; He, Chen, & Evans, 2007). Although brain networks can be constructed using other neuroimaging techniques, including functional magnetic resonance imaging (fMRI) and diffusion tensor imaging (DTI) (Alonso Montes et al., 2015; Diez et al., 2015), MBNs have many distinct advantages from being constructed using T1-weighted images, an imaging modality that is routinely acquired in clinical settings and has a high signal-to-noise ratio, the preprocessing pipeline is much simpler and does not require the removal of physiological noise; furthermore, movement artifacts are small (H. Wang, Jin, Zhang, & Wang, 2016; Wang, Jiao, & Li, 2020). Given that morphological measures, especially gray matter volume, have specific neurological and genetic bases, MBNs reflect the level of synchronous maturation between anatomical regions during brain development (Alexander-Bloch, Giedd, & Bullmore, 2013). Converging evidence suggests that group-level MBNs using structural covariance exhibit specific network patterns (Duan et al., 2020; Lim, Jung, & Aizenstein, 2013; Yun et al., 2020; Zou, She, Zhan, Gao, & Chen, 2018). Duan et al. (2020) reported a decrease in long-range structural covariance and an increase in structural covariance in subcortical structures in ASD, suggesting the crucial role of aberrant synchronized maturation between subcortical regions in social cognition and behavior in ASD. Nevertheless, only one MBN was created for a specific group of participants, thereby ignoring interindividual differences (Saggar et al., 2015). Several techniques have been developed to directly extract structural information from T1-weighted images and construct individual-based MBNs that can reflect developmental coordination among anatomical regions at the individual level (Kong et al., 2015; Raj, Mueller, Young, Laxer, & Weiner, 2010; Tijms, Seriès, Willshaw, & Lawrie, 2012; Zhou et al., 2011). Kong and colleagues presented a method to estimate interregional morphological connectivity by using the Kullback–Leibler (KL) divergence without ignoring remarkable inter-subject variability in the geometry (e.g., shape and size) among different brain regions (Kong et al., 2014; Kullback & Leibler, 1951). Exploring such individual-based MBN organization may allow for the sensitive detection of subtle brain maldevelopment under pathological conditions.

Autism spectrum disorder (ASD) is a childhood-onset atypical neurodevelopmental condition causing deficits in social communication, social reciprocity, and restricted and repetitive behaviors (RRBs) (Association American Psychiatric, 2013). Accumulating evidence suggests that ASD is accompanied by atypical structural brain connectivity within the neural systems related to social deficits (Billeci, Calderoni, Tosetti, Catani, & Muratori, 2012; Im et al., 2018; Noriuchi et al., 2010) that is majorly referred to connectivity based on DTI (Chung, Adluru, Dalton, Alexander, & Davidson, 2010; Chung, Adluru, Dalton, Alexander, & Davidson, 2011; Dennis et al., 2011; He et al., 2020). One study found that the decreased fractional anisotropy (FA), a metric of white matter integrity, of the inferior longitudinal fasciculus is negatively correlated with social interaction in ASD (Im et al., 2018). Another report showed a negative association with social impairment of FA in the left dorsolateral prefrontal cortex, implying that abnormalities in fiber tract integrity are associated with social deficits in ASD (Noriuchi et al., 2010). However, genetic and molecular studies revealed that abnormal neural connectivity in individuals with ASD may not be necessarily constrained only by white-matter connectivity but also by direct synaptic connections within gray matter (Abell et al., 1999; McAlonan et al., 2005). Some abnormalities in the gray matter of young children with autism were discovered to be the underlying developmental mechanisms of brain and behavior (Gori et al., 2015; J. Liu et al., 2017; Sparks et al., 2002). A recently developed group-wise anatomical covariance network of brain gray matter in young children with autism revealed that abnormally topological properties favor local rather than global network interactions (Bethlehem, Romero-Garcia, Mak, Bullmore, & Baron-Cohen, 2017), thus enabling its prediction for social communication deficits (Duan et al., 2020). Although morphological gray matter networks provide valuable information regarding synchronized gray matter maturation during brain development (Alexander-Bloch et al., 2013; Evans, 2013), the construction of these networks in an individual level remains largely unexplored. Hence, this work constructed individual-based gray matter networks to explore specific

morphological network patterns related to social deficits in young children with ASD. In particular, individual ROI-wise MBNs were assessed based on gray matter volume from anatomical MRI to identify specific network patterns. Predictive models were also established to unveil the association between network patterns and social impairment severity. This study provides answers to the following two questions: (a) whether young children with ASD exhibit more serious abnormal topological properties in MBNs compared with TDC; and (b) whether the discovered abnormal morphological connectivity patterns constitute a potential neuromarker for estimating social deficits.

2 | MATERIALS AND METHODS

2.1 | Participants

This study included 40 young children with ASD recruited from Sichuan Provincial Rehabilitation Hospital (Chengdu, China) and 38 age-, gender-, and handedness-matched typically developing children (TDC) recruited from the local kindergartens through advertisements. Patients were excluded if at least one of the following conditions occurred: (a) have a genetic etiology of ASD (e.g., fragile X syndrome and 15q syndrome); (b) have history of seizure disorders and/or attention deficit hyperactivity disorder; (c) have history of loss of consciousness for >5 min and/or current medication with psychoactive drugs, and (d) have history of brain injury or other psychiatric neurological disorders. All TDC did not have any neurological disorders as assessed by the Structured Clinical Interview for Diagnostic and Statistical Manual of Mental Disorders (DSM-V) Axis | Disorders-non-patient version nor a family history of psychiatric illness in any first-degree relative. Detailed clinical and demographic data are shown in Table 1.

After the full explanation on the purpose of this study, written informed consents were acquired from all participants' parents or legal representants. This work was approved by the research ethical committee of University of Electronic Science and Technology of China and Sichuan Provincial Rehabilitation Hospital and has been registered at https://clinicaltrials.gov/ (Identifier: NCT02807766).

2.2 | Diagnosis and clinical assessment

Patients with ASD were diagnosed by experienced psychiatrists using the fifth edition of the DSM checklist with a series of clinical assessments focusing on detailed developmental history, clinical observation, and cognitive condition (Association American Psychiatric, 2013). Among them, 23 were evaluated by the Autism Diagnostic Observation Schedule (ADOS) (Lord et al., 2000), and 17 could not be evaluated due to the unwillingness of parents or representants or the lack of children's cooperation. ADOS provides a semi-structured, interactive autism diagnostic observation to assess autistic symptoms. Each ADOS subdomain is scored on a four-point scale, and high scores indicated high symptomatic severity.

The TDC were assessed for verbal IQ, performance IQ, and full-scale IQ by using the Wechsler Intelligence Scale for Children

TABLE 1 Participant demographics

	ASD (n = 40)	TDC (n = 38)			
	Mean ± *SD*	Mean ± *SD*	t/x^2	p-value	Effect size
Age (years)	5.25 ± 1.10	5.64 ± 0.85	$t_{(76)} = 1.72$	$p = .09$[a]	0.39
Age range (years)	3.6–7.6	2.7–6.8	–	–	
Sex (male/female)	32/8	28/10	$\chi^2 = 0.44$	$p = .51$[b]	0.14
Handedness (right/left/mixed/N/A)	30/3/3/4	35/1/2/0	$\chi^2 = 1.53$	$p = .46$[b]	0.28
Image quality scores (3/4/5)	7/20/13	9/12/17	$\chi^2 = 2.73$	$p = .25$[b]	0.38
ADOS					
Communication	6.17 ± 1.90	–	–	–	
Social interaction	10.13 ± 3.35	–	–	–	
Communication + social interaction	16.30 ± 4.86	–	–	–	
Stereotyped behaviors and restricted interests	1.70 ± 1.58	–	–	–	
IQ					
Full scale IQ	–	111.25 ± 10.05	–	–	
Performance IQ	–	105.07 ± 15.34	–	–	
Verbal IQ	–	108.82 ± 12.39	–	–	

Note: Effect size, a statistical metric that measures the strength of the relationship between two variables on a numeric scale. ADOS was unavailable for 17 children with ASD. $t(df)$, Between-group t statistic and degrees of freedom.

Abbreviations: ADOS, autism diagnostic observation schedule; ASD, autism spectrum disorder; IQ, intelligence quotient; *SD*, standard deviation; TDC, typically developing children.

[a]p-value obtained by two-sample t test.

[b]p-value obtained by the Kruskal–Wallis test.

(WISC-IV) to further exclude children with mental retardation (Olivier, Mahone, & Jacobson, 2018; Wechsler, 1949). Assessing the IQ of young children with ASD using WISC-IV is difficult due to their substantial language impairments. Thus, the subjects with ASD did not undergo an IQ assessment.

2.3 | Data acquisition

MRI data were acquired in all participants using a 3 Tesla GE DISCOVERY MR750 scanner (General Electric, Fairfield Connecticut) with a high-speed gradient and an eight-channel prototype quadrature birdcage head coil at University of Electronic Science and Technology of China. Foam padding was utilized to reduce head motion for all participants. During scanning, the TDC group was instructed to keep still and watch cartoons, and the ASD group was sedated using 50 mg/kg chloral hydrate (CH) under a strict clinical protocol established by the Radiology Sedation Committee of the hospital. CH was frequently used as a sedative and hypnotic pharmaceutical drug, has a long history of safety and availability in infants, and is used commonly for pediatric electroencephalography sedation (Jan & Aquino, 2001; Rumm, Takao, Fox, & Atkinson, 1990). Mild to moderated doses of CH do not affect neural responses, and 80 mg/kg CH is set as the maximum dose to ensure the relatively low risk of unwanted side effects (Avlonitou et al., 2011; Sisson & Siegel, 1989). Therefore, CH may not disturb these findings in this study. Finally, each kid's guardian was present during scanning.

High-resolution MR images were obtained using a 3D T1 sequence with the following acquisition parameters: repetition time/echo time (TR/TE) = 6.02/1.96 ms, 156 slices, 256 × 256 matrix, 7° flip angle, field of view = 256 mm × 256 mm, and voxel size = 1 mm × 1 mm × 1 mm. Each T1 image was manually inspected for motion artifacts by three experienced personnel. Image quality was estimated using five scores ranging from 1 (indicating poor quality) to 5 (good quality). Images were excluded only when the average score across evaluators was less than or equal to two points. A second inspection was then performed based on the homogeneity in voxel-based morphometry maps. After the normalized segmented gray matter (GM) map was obtained for each subject (detailed description in the following MR image preprocessing section), Pearson's correlation between normalized GM maps was calculated, and a correlation matrix was then generated ($N * N$, N is total number of subjects). The homogeneity of each subject was defined as the average of each row of the correlation matrix. GM maps with low homogeneity (less than mean-2*SD of the GM maps) were manually checked again. The homogeneity of segmented GM maps between subjects was calculated by using a Computational Anatomy Toolbox (CAT12, http://www.neuro.uni-jena.de/cat/).

2.4 | Data analysis

2.4.1 | MRI preprocessing

T1-weighted images were preprocessed using the Computation Anatomy Toolbox (CAT 12; Christian Gaser; Department of Psychiatry, University of Jena) implemented in Statistical Parametric Mapping (SPM 12; Wellcome Department of Cognitive Neurology, University of London, UK) for voxel-based morphometry (VBM) analysis to obtain voxel-wise gray matter volumes for each subject. All T1-weighted images from ASD and TDC groups were first corrected for bias-field inhomogeneities and then segmented into gray matter (GM), white matter (WM), and cerebrospinal fluid (CSF) by using the customized pediatric tissue probability maps generated with the Template-O-Matic 8 toolbox (TOM8, http://dbm.neuro.uni-jena.de/wordpress/software/tom/). During segmentation, a hidden Markov Random Field model was applied to account for partial volume effects (Cuadra, Cammoun, Butz, Cuisenaire, & Thiran, 2005; Tohka, Zijdenbos, & Evans, 2004). The segmented images from ASD and TDC groups were spatially normalized using the DARTEL algorithm (Ashburner, 2007) to create the gray matter template for the cohort through iterative registration. Finally, the resulting scans were smoothened using a Gaussian kernel of 8 mm full width at half maximum (FWHM). Total intracranial volume (ICV), calculated as the sum of GM, WM, and CSF volumes, was used as a covariate for further statistical analyses.

2.4.2 | Construction of individual MBN

Large-scale MBNs for each participant were constructed based on their GM volume images (Figure 1). Herein, network nodes represent brain regions defined by the automated anatomical labeling (AAL) atlas, which included 90 brain regions (Tzourio-Mazoyer et al., 2002), and network edges were quantified by the symmetric KL divergence-based similarity (KLS) (Kong et al., 2014; Kong et al., 2015; Wang et al., 2016) and defined as:

$$KLS(P,Q) = e^{-D_{kl}(P,Q)}, \quad (1)$$

a measure between 0 and 1, where 0 indicates the maximum separability between the gray matter P and Q density distributions, and 1 is for two identical distributions. Equation (1) uses the KL distance, that is,

$$D_{KL}(P,Q) = \sum_{i=1}^{n}\left(P(i)log\frac{P(i)}{Q(i)} + Q(i)log\frac{Q(i)}{P(i)}\right), \quad (2)$$

where n is the total number of sample points ($n = 2^7$ was used in this study, similar to the one in Wang et al., 2016). P and Q were estimated for each node using a kernel density estimation (Botev, Grotowski, & Kroese, 2010). One KLS-based MBN (i.e., 90 × 90 similarity matrix) was generated for each participant, and the averaged network across the participants was averaged. An average linkage clustering method was applied to the elements in the averaged MBNs to investigate whether such hierarchical organization is present in MBNs across participants (Eisen, Spellman, Brown, & Botstein, 1998) (Figure 2). The coefficient of variation map (CV, ratio of the *SEM*) was

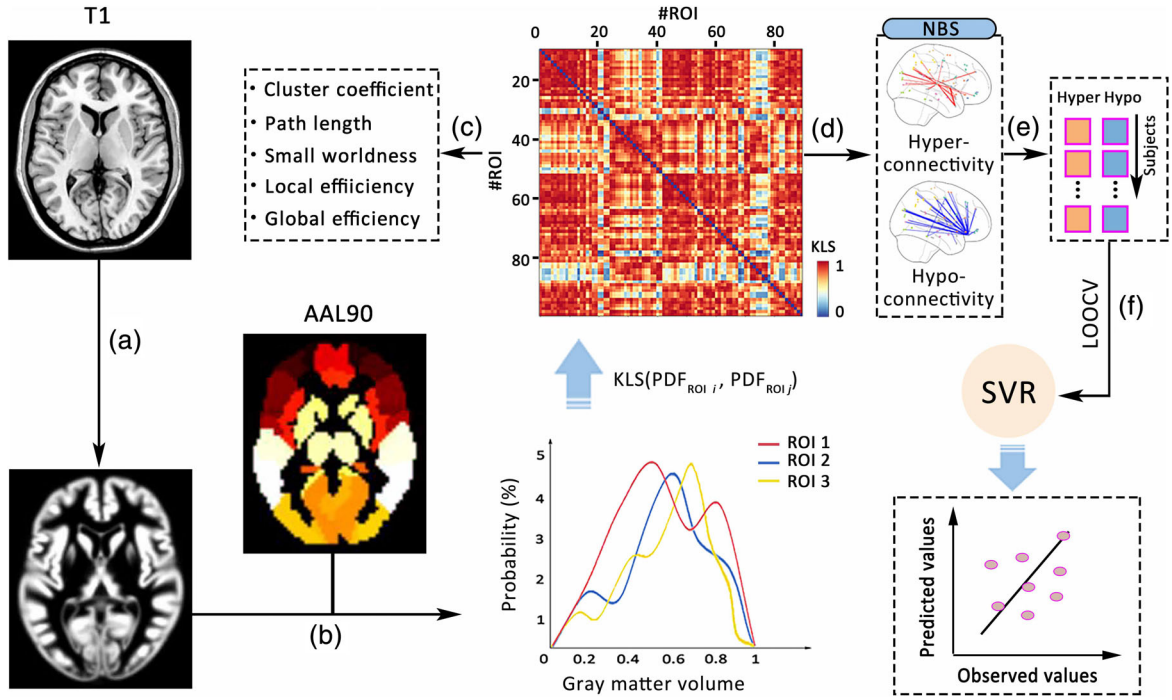

FIGURE 1 Overview of methodological sketch. (a) Estimation of gray matter volume using a standard VBM procedure. (b) Brain parcellation with the AAL90 atlas and construction of individual morphological network using similarity (i.e., KLS) between PDFs from different brain regions. c) Calculation of network metrics. (d) Exploration of abnormally morphological subnetworks using the NBS technique. (e) Construction of features based on the average from connections in each subnetwork. (f) Estimation of symptomatic severity using SVR model built on LOOCV. Note that the KLS matrix was generated from the brain network organization of one subject. VBM, voxel-based on morphometry; AAL, anatomical automatic labeling atlas; ROI, region of interest; KLS, Kullback–Leibler divergence-based similarity; PDF, probability density function; NBS, network-based statistic; SVR; Linear support vector regression; and LOOCV, leave-one-out cross validation

also calculated to show the consistency of the connections in the network across participants (Kong et al., 2015) (Figures S1 and S2).

2.5 | Graph theory analysis

2.5.1 | Threshold selection

To validate the topological properties of the derived morphological connectivity matrices, each matrix was thresholded into a set of weighted networks, by using the desired sparsity for noisy element exclusion. Nodes represented brain regions, and edges represented undirected connections. Connectivity sparsity S (i.e., the ratio of the existing edges to the maximum possible number of edges in the network) was used as a threshold measurement to ensure the same number of nodes and edges in the resultant networks across participants and complete the comparison of between-group differences in network organization (Achard & Bullmore, 2007). Instead of selecting a single threshold, a consecutive sparsity range of $0.05 < S < 0.4$ (interval = 0.02) was employed to each weighted matrix (Achard, Salvador, Whitcher, Suckling, & Bullmore, 2006; He et al., 2007; Watts & Strogatz, 1998). All the following network analyzes were performed repeatedly using a different threshold value among all possible ones.

2.5.2 | Network metrics

MBNs at different sparsity threshold S were assessed by calculating global network metrics using the GRETNA toolbox, which include small-world parameters (i.e., weighted clustering coefficient C^w, weighted characteristic path length L^w, normalized weighted clustering coefficient γ, normalized weighted characteristic shortest path length λ, and small-worldness σ) and network efficiency (i.e., local efficiency E_{local} and global efficiency E_{global}) (Duan et al., 2014; Jinhui Wang et al., 2015). Detailed descriptions of the above metrics are shown in Supplementary Information. Area under the curve (AUC) was computed for each network metric Y to provide a summarized scalar for the topological characterization of brain networks and was expressed as follows:

$$Y^{AUC} = \sum_{k=1}^{n-1} [Y(S_k) + Y(S_{k+1})]\Delta S/2. \quad (3)$$

Sparsity thresholds were varied from $S_1 = 0.05$ to $S_n = 0.4$ with step variations of $\Delta S = 0.02$. The AUC metric has been applied in prior studies and enables the sensitive detection of topological alterations in some diseases (Zhang et al., 2011).

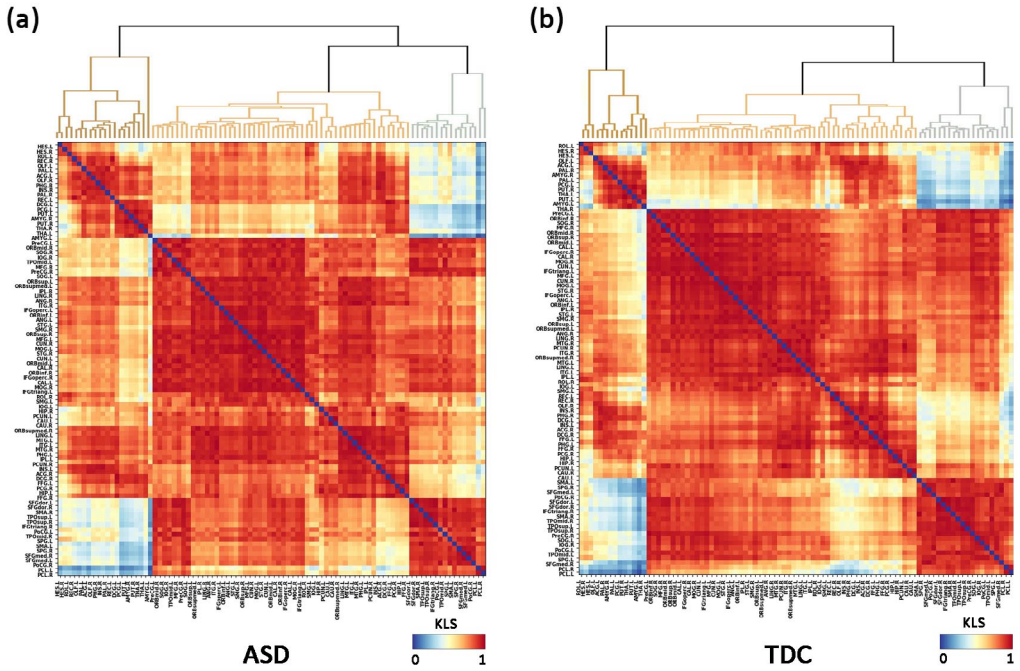

FIGURE 2 Averaged MBNs across participants in ASD (a) and TDC (b). Red and blue color represent high and low similarity values between ROIs, respectively. Principal diagonal values (i.e., self-connection) were excluded from the following analyses and thus fixed to zero. The rows and columns were reordered based on the labels obtained after hierarchical clustering, which allows visualizing together those ROIs with great similarity between pairs. Clustering hierarchy was displayed on top of the matrices by using dendrograms. MBNs, morphological brain networks; ASD, autism spectrum disorder; TDC, typically developing control. L, left; R, right

2.6 | Statistical analysis

2.6.1 | Between-group differences

Nonparametric permutation tests were conducted on the network metrics, that is, small-world and network efficiency, to determine the differences in the network properties between ASD and TDC (Bullmore et al., 1999). First, between-group differences in each network metric in the specific threshold and its corresponding AUC across the defined range of sparsity thresholds were calculated. All the values were then randomly shuffled into two groups, and the mean differences between the two randomized groups were recalculated to reject the null hypothesis that the existing group differences could be caused by chance. This permutation procedure was repeated 10,000 times, and the 95th percentile of each distribution provided the significant values with a possibility of type I error of 0.05. False discovery rate (FDR) was applied to correct multiple comparisons (Benjamini & Hochberg, 1995). Multiple linear regression analyses were performed before the permutation tests to eliminate the confounding effects of ICV and gender for each network metric. Moreover, network-based statistics (NBS) was employed to localize regional brain networks indicating significant between-group differences in inter-regional morphological connectivity (Zalesky, Fornito, & Bullmore, 2010). Two sample t test statistics was employed to weigh for each edge, and those with $t > 3.42$ (corresponding to $p < .001$, uncorrected) were systematically searched for connected edges with the same effect. Interconnected networks, formally known as graph components, were then determined. A family-wise error (FWE) corrected p value was computed for the size of each resulting component by using a nonparametric permutation approach (1,000 permutations). For each permutation, the group labels were randomly shuffled, and the size of the largest interconnected network was determined to yield an empirical estimate of the null distribution of maximal component size. A FWE-corrected p value was evaluated for each interconnected network as the proportion of permutations yielding a relatively large or equal-sized interconnected network. Before NBS, multiple linear regression analyses were conducted to remove the effects of nuisance variables (i.e., ICV and gender). Finally, the NBS identifies the connected subnetwork(s) that differ the most between groups. In addition, 4,005 morphological connections (4,005 [$90 \times (90–1)/2$] referring to the total number of connections in MBN) were compared between ASD and TDC, and these morphological connections showing between-group differences were correlated with age in the ASD group to further explore whether the atypically morphological connectivity associated with brain development exhibits a specific connectivity pattern. ICV and gender also served as nuisance covariates.

2.6.2 | Prediction of autistic symptoms

A linear support vector regression (SVR) was applied to estimate each patient's symptom severity scores based on the mean of the strength of all edges in each connected subnetwork to further investigate

whether the connected subnetwork(s) obtained from NBS can predict the severity of ASD symptoms. Two classes of connected subnetworks, namely, hyper-connected and hypo-connected networks were used. Leave-one-out cross validation (LOOCV) approach, which is known to avoid overfitting in the regression model, was adopted in this work (Rosenberg et al., 2016; Shen et al., 2017). For LOOCV, the estimated values from "left-out" subjects were obtained by extracting the training data from all other subjects and repeating this procedure until all subjects had an estimated value. The correlation between the scores of estimated and observed symptoms were then calculated while controlling for ICV and gender. Its statistical significance was examined using permutation tests. In each permutation, the group labels were reallocated, and the same regression procedure was repeated to obtain a R_{perm} value based on each reallocated dataset. This permutation procedure was repeated 10,000 times, and the final p value was generated by the proportion of the number of times that R_{perm} is larger or equal to the actual R-value in total permutation times.

2.7 | Reproducibility analysis

The robustness of our findings was first validated using interval = 0.01 and 0.03 across the range of sparsity thresholds. Data were then reanalyzed while controlling for nuisance variances of ICV, age, and gender to examine the result robustness with regression of age (ROA). Finally, the widely applied K-fold cross-validation strategy (i.e., K = 10) was employed to further examine the reliable results by using different cross-validation techniques (Aghdam, Sharifi, & Pedram, 2018; Shen et al., 2017).

3 | RESULTS

3.1 | Attenuated small-worldness of MBNs in ASD

The averaged MBNs for ASD and TDC group are shown in Figure 2a, b, respectively. Specific connectivity patterns for each group were assessed by hierarchical clustering. Most connections with relatively high similarity exhibited relatively low CV (Figures S1 and S2), and this phenomenon occurred with a high consistency across subjects. Compared with those in TDC, the MBNs in individuals with ASD exhibited significantly lower σ and γ in each sparsity threshold and their corresponding AUC (σ, p = .011, γ, p = .009, Figure 3a,b, FDR corrected) across the defined range of sparsity thresholds. Although the significant differences in σ and γ were observed between ASD and TDC, the MBNs in young children with ASD did not exhibit small-world topological organization because they did not satisfy the

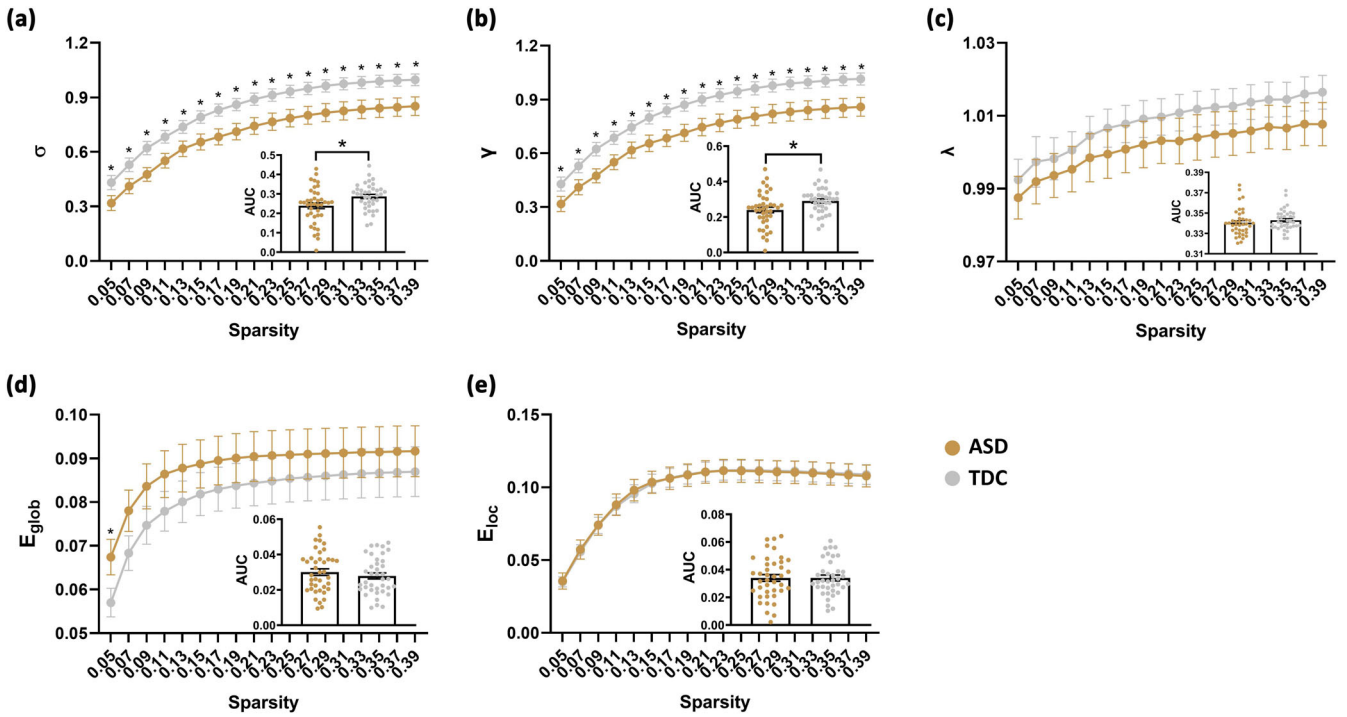

FIGURE 3 Between-group differences in the global topological metrics of MBNs between ASD and TDC. (a) Group differences in σ for different values of sparsity threshold. Gold and silver curves represent σ values in ASD and TDC, respectively. Inset maps show group differences in AUC for σ across the different sparsity thresholds. Error bars indicate *SEM*. Similar to panel (a) but for (b) γ, (c) λ, (d) E_{glob}, and (e) E_{loc}. Asterisks indicate significance level of p < .05 (FDR corrected). MBNs, morphological brain networks; σ, small-world topology; γ, normalized clustering coefficient; λ, normalized characteristic shortest path length; E_{glob}, global efficiency; E_{loc}, local efficiency; AUC, area under the curve; FDR, false discovery rate. ASD, autism spectrum disorder; TDC, typically developing control

conditions (i.e., $\sigma = \gamma/\lambda$, $\gamma > 1$ and $\lambda \approx 1$) in Figure 3. Considering the scalar quantitative measurement of σ ($\sigma = \gamma/\lambda$) and lack of significant difference in λ ($p > .05$, Figure 3c), we speculated that the decreased small-worldness (σ) can be attributed to the decreased normalized clustering coefficient (γ) in young children with ASD. In relation to network efficiency metrics, no significant differences were found in global (E_{global}, $p > .05$, Figure 3d) or local (E_{local}, $p > .05$, Figure 3e) efficiency.

3.2 | Network-based statistics identified two impaired morphological connectivity subnetworks

NBS identified two impaired morphological subnetworks, one characterized by hyper-connectivity and the other one by hypo-connectivity based on KLS. The hyper-connectivity network consisted of 35 connections and affected subcortical structures such as thalamus, pallidum, and putamen, and cortical regions that together formed the cortico-striatum-thalamic-cortical (CSTC) circuitry (Figure 4a). Meanwhile, the hypo-connectivity network comprised 60 connections that majorly affect cortical regions, including short-distance connections within the prefrontal cortex and long-distance connections linking different lobes, and referred here as cortico-cortical networks (Figure 4b). Age-related atypical connectivity pattern, which is sensitive to brain development, was also distinguished from the impaired morphological subnetworks (Figure S3).

3.3 | Abnormal connectivity in MBNs predicts symptom severity in ASD

With the use of a linear SVR approach, the abnormal hyper-connectivity and hypo-connectivity networks obtained from NBS were found to predict communication deficits ($p = .035$, permutation test, Figure 5) but not abnormal social reciprocity (Figure S4) and RRB (Figure S5) in young children with ASD.

3.4 | Reproducibility of findings

Consistent results were found with given interval = 0.01 (Figure S6) and 0.03 (Figure S7) in the defined range of sparsity thresholds, suggesting that these findings are independent of the parameter of interval. Despite the missing few connections in connected subnetworks and weak statistical significance of topological properties

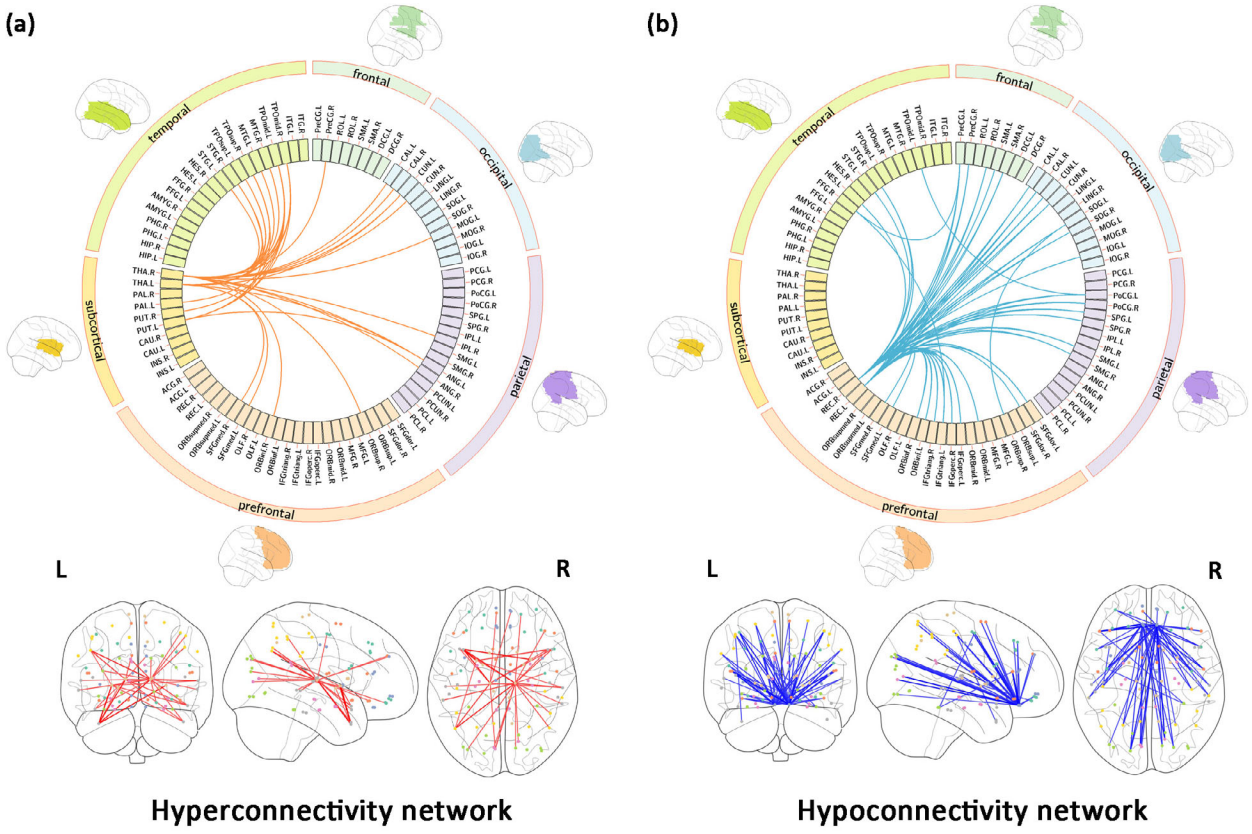

FIGURE 4 Hyperconnectivity (a) and hypoconnectivity (b) networks identified by NBS. (a) Hyperconnectivity network consisted of 35 interconnected links represented by red lines in top wheel and bottom glass-brain. Different ROIs from the AAL90 anatomical atlas were grouped in six different networks as shown in the wheels with brain plots and with a different color. (b) Hypoconnectivity network consisted of 60 interconnected links (i.e., blue lines). NBS, network-based statistic; AAL, anatomical automatic labeling atlas; ROI, region of interest; ASD, autism spectrum disorder; TDC, typically developing control; L, left; R, right

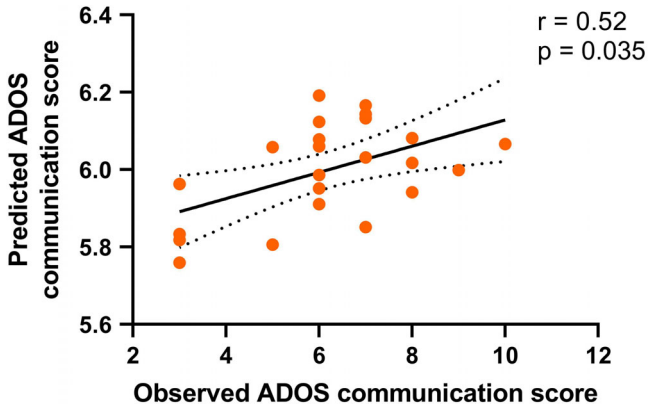

FIGURE 5 Correlation between predicted and observed values in the ADOS communication subscore in ASD. Solid and dashed lines denote respectively the best-fitted line and 95% confidence interval of the Pearson's correlation analysis. ADOS scores could not be obtained for 17 ASD kids. ADOS, autism diagnostic observation schedule; ASD, autism spectrum disorder

relative to our main results, consistent results were observed even when ROA was applied (Figures S8, S9, and S10), suggesting the minimal effect of ROA on our findings. In the 10-fold cross-validation analysis, a marginal significant association was found between predicted and observed ADOS communication score after the permutation test (p = .06, 10,000 times, Figure S11). In summary, these analyses performed well with different conditions, the findings are robust.

4 | DISCUSSION

Individual-based MBNs were built using structural MRI data to systematically identify altered morphological connectivities and their relationship to social behavior in young children with ASD. The findings can be summarized as follows: (a) young children with ASD exhibited significantly decreased values of σ due to a decrease in the normalized clustering coefficient; and (b) the discovered impaired morphological connectivity patterns, namely, increased connectivity in the CSTC circuitry and decreased connectivity in the cortico-cortical network, predicted the severity of social communication deficits in childhood autistic brain. All these results suggest that the individual-based morphometry approach provides a new window for interpretation of human brain anatomical networks a.k.a., human connectome. Novel measurements assessing morphological network patterns, which can underline behavioral impairment in ASD, might also define a new class of putative biomarkers that aid in the diagnosis of autistic symptoms.

4.1 | Delay to establish efficient MBN in the infantile autistic brain

The human brain is a complex network where a multitude of short-range and long-range connections coexist, and its efficiency in segregating and distributing information is characterized by topology properties (e.g., small-worldness) (Bassett & Bullmore, 2017; Power, Fair, Schlaggar, & Petersen, 2010; Watts & Strogatz, 1998). The topology properties of the brain network are age-dependent, and the brain network reaches an adult-like topological organization via substantial changes in brain connectivity and development of specific brain function (Cao et al., 2017; Gao et al., 2011). Although the topological configuration of MBNs in young children with ASD and TDC did not exhibit based on the definition of small-worldness, we speculate that MBNs would shift from a random arrangement toward an ordered configuration and be established into the high-efficient organization for information processing during maturation. Moreover, brain maturation results from a combination of pruning redundant connectivity and strengthening synergistic connectivity to provide an efficient whole-brain network organization, that is, assembling highly interconnected networks with low cost (E. Bullmore & Sporns, 2012; Supekar, Musen, & Menon, 2009). The cluster coefficient (i.e., γ) is an indicator of local network interconnectedness, and the path length is a measure of its overall connectedness; these two are the key components of small-worldness (Watts & Strogatz, 1998). Here, the significantly lower values of σ and γ in young children with ASD than in TDC suggest the delay in establishing efficient brain morphological organization in an autistic developing brain. A possible cause is the impaired pruning in the local connections during development, but this statement needs further investigation. Although the absence of the small-worldness in MBNs is inconsistent with fMRI and DTI studies suggesting a continued development of the small-worldness in the infantile brain (Fair et al., 2009; Power et al., 2010; Van Den Heuvel et al., 2015), the present findings may provide complementary information on topological configuration during the development of the brain network by using T1 imaging data.

4.2 | Increased morphological connectivity in the CSTC circuitry in ASD

The findings indicated an increased morphological connectivity in CSTC circuitry, which involves the thalamus, striatum, pallidum, and cerebral cortex (especially in temporal lobe) (Figure 4a) (Gunaydin & Kreitzer, 2016; Maximo & Kana, 2019). CSTC plays a critical role in auditory information processing related to social context, during which the basal ganglia (mainly in striatum and pallidum) integrate excitatory signals from the cortex to be sent back to other cortical regions via thalamic projections (Fuccillo, 2016; Gunaydin & Kreitzer, 2016; Hilton et al., 2010). Accumulating evidence suggests that individuals with ASD show heightened auditory sensitivity and atypical responses and filtering to complex auditory stimuli (Hilton et al., 2010; Matsuzaki et al., 2012). Autistic brains were recently discovered to exhibit increased auditory–thalamic connectivity in ASD (Maximo & Kana, 2019) and auditory–basal ganglia connectivity, majorly between superior temporal gyrus and putamen (Di Martino et al., 2011). Gunaydin & Kreitzer, 2016) reported that the exiting downstream projection patterns between basal ganglia and thalamus

are composed of GABAergic medium spiny neurons and suggested that inhibitory mechanisms might mediate such control in human behavior. In agreement with previous studies, the current findings supported that the strengthened morphological integration in the CSTC circuit may be associated with the altered ability of auditory information processing in an autistic developing brain.

4.3 | Decreased cortico-cortical MBNs in childhood autistic brain

Young children with ASD exhibited a decrease in cortico-cortical MBNs, which involve prefrontal, frontal, parietal, and occipital lobes (Figure 4b). A weak connectivity of cortical networks has been found in ASD (Cherkassky, Kana, Keller, & Just, 2006; Just, Cherkassky, Keller, & Minshew, 2004; Murias, Webb, Greenson, & Dawson, 2007). A positron emission tomography study also showed a weak association between glucose metabolic levels in frontal and posterior brain regions in individuals with ASD (Horwitz, Rumsey, Grady, & Rapoport, 1988). Another single-photon emission computed tomography research found that young children with ASD exhibit delay in the maturation of frontal lobe circuitry compared with control participants (Zilbovicius et al., 1995). A recent MRI research proposed the cortical hypo-connectivity theory in ASD (Just et al., 2004; Just, Cherkassky, Keller, Kana, & Minshew, 2007; Kana, Libero, & Moore, 2011). This theory assumes an inefficient interregional brain connectivity across the cerebral cortex that results in abnormal information integration at psychological and neural levels in autistic brains and may also explain diverse impairments in social symptoms (Just et al., 2004; Schipul, Keller, & Just, 2011). Other studies also revealed that the overall connectivity class in ASD is highly heterogeneous, and a combination of hyper- and hypo-connectivity seems to coexist across different subtypes of ASD (Maximo & Kana, 2019; Rasero, Jimenez-Marin, Diez, Hasan, & Cortes, 2020; Yerys et al., 2017) and trajectories of neural development (C. He et al., 2020).

Social interactions largely rely on information integrative processing, which requires a compromise of high-quality interaction and efficiently recurrent cognitive processing during human interaction. Given that understanding, another person's mind requires high-level abstraction, the deficit in the theory of mind could be due to abnormal integrative social and cognitive processing, thus extending the theory of hypo-connectivity to all cognitive and social profiles in autism (Baron-Cohen, Leslie, & Frith, 1985). Furthermore, a decrease in synchronization among brain regions while performing a working memory task was found in individuals with ASD (Koshino et al., 2005). Other authors found that autistic participants showed lower functional connectivity among the frontal, parietal, and occipital lobe compared with healthy controls (Damarla et al., 2010). This finding supported the hypo-connectivity theory in ASD to explain social and cognitive impairments in this condition (Just et al., 2004; Schipul et al., 2011). The present results also consistent with the hypo-connectivity theory and suggest that the decreased cortico-cortical morphological connectivity may be associated with the complex cognitive and social functions in ASD. On the basis of similar functional abnormalities in previous reports (Kana et al., 2011; Maximo & Kana, 2019), the two paired MBNs in the current work in may facilitate the combination of morphological information (i.e., coordination of gray matter structure) and functional interaction in the two subnetworks in ASD. These findings help in understanding the physiological meaning of MBNs via functional imaging evidence and further agree that the brain structure provides support to its functional information processing (Park & Friston, 2013).

4.4 | Association of the abnormalities in MBNs with communication deficits in ASD

The observed abnormalities in morphological connectivity patterns such as increased connectivity in CSTC and decreased connectivity in the cortico-cortical network can be used to predict the severity of communication deficits in childhood ASD. This finding may reflect that the aberrant integration of information has a behavioral manifestation in the social-communicative domain of young children with ASD. This brain–behavior association also underscores the potential importance of abnormally morphological connectivity in CSTC circuitry and across the cerebral cortex in ASD. These results are consistent with prior studies supporting the potential relationships between atypical social information processing and brain connectivity including structural connectivity (Duan et al., 2020) and functional connectivity (Gotts et al., 2012; Guo et al., 2020) in ASD.

4.5 | Limitations

Our findings should be considered in light of some limitations. First, 17 children with ASD were absent of assessment with ADOS, due to the unwillingness of the guardians or uncooperation of children during the evaluation. Future studies utilizing a large sample size with completely clinical phenotype assessment are needed to generalize the current results to a broad population with ASD. Second, young children with ASD were sedated using CH to reduce motion artifacts and ensure a complete MRI examination. Stringent quality control and inclusion criteria (e.g., rating of imaging quality and homogeneity of gray matter maps) were also used. Although CH has been used in many studies of gray matter (Liu et al., 2019; Jia Wang et al., 2017), evidence disproving the influence of CH on gray matter remains insufficient. Further works must explore the exact effect of CH on gray matter. Third, the morphological connectivity in this study was built from the probability distributions of morphological variables obtained from structural neuroimaging. Such distributions require an accurate evaluation. In this study, regions of interest have been defined from the AAL atlas widely used for brain network constructions (Gong et al., 2009; Zhang et al., 2011). This atlas exhibited sufficiently large observations for each brain area (larger than 120) and ensured the accurate evaluation of regional morphological distributions. However, previous studies with either resting-state fMRI or diffusion MRI have reported that measuring network properties (e.g., small-world properties) possibly rely on the choice of the brain template to some extent.

A comparison of the present results with those obtained using different templates is important to offer comprehensive insights into the effect of different brain parcellation schemes on the topological organization of individual-level morphological brain networks. Fourth, although a reliable ROI-wise morphological connectivity has been achieved by the KLS technique (Kong et al., 2015; Wang et al., 2016; Zhao et al., 2020), additional experiments are still required to identify the extent of how morphological connectivity can reflect structural or functional connectivity. Several similarity and dissimilarity metrics (i.e., wavelet-based and correlative features) can be adopted to evaluate morphological connectivity in future studies. Constructing individual morphological networks and investigating how they are affected by other factors, such as cortical thickness, area and curvature, tissue density, or cell type derived in the native space are of particular importance.

5 | CONCLUSION

Young children with ASD exhibited poor efficiency of individual-level morphological brain networks, and the abnormal morphological connectivity patterns (i.e., increased connectivity in CSTC circuitry and decreased connectivity in cortico-cortical network) are substantially associated with social communication deficits. These results suggest the critical contribution of aberrant morphological network patterns to the neuropathology of ASD. A thorough description of the specific morphological brain network is required for a sufficient understanding of ASD pathogenesis and behavioral symptoms.

ACKNOWLEDGMENTS

This work was supported by the National Natural Science Foundation of China (Nos. 81871432, U1808204, and 62036003), the Sichuan Science and Technology Program (2019YJ0180), and the Fundamental Research Funds for the Central Universities (Nos. 2672018ZYGX2018J079, ZYGX2019Z017). JMC acknowledges financial support from Ikerbasque: The Basque Foundation for Science and from Ministerio de Economia, Industria y Competitividad (Spain) and FEDER (grant DPI2016-79874-R). Heng. C also acknowledges financial support from National Natural Science Foundation of China (61901129) and China Postdoctoral Science Foundation (2019M660236).

CONFLICT OF INTEREST

The authors declare no conflict of interest.

DATA AVAILABILITY STATEMENT

This work was approved by the research ethical committee of University of Electronic Science and Technology of China and Sichuan Provincial Rehabilitation Hospital and has been registered at https://clinicaltrials.gov/ (Identifier: NCT02807766).

ORCID

Xujun Duan https://orcid.org/0000-0001-8543-2117

REFERENCES

Abell, F., Krams, M., Ashburner, J., Passingham, R., Friston, K., Frackowiak, R., & Frith, U. (1999). The neuroanatomy of autism: A voxel-based whole brain analysis of structural scans. *Neuroreport*, *10*(8), 1647–1651.

Achard, S., & Bullmore, E. (2007). Efficiency and cost of economical brain functional networks. *PLoS Computational Biology*, *3*(2), e17.

Achard, S., Salvador, R., Whitcher, B., Suckling, J., & Bullmore, E. (2006). A resilient, low-frequency, small-world human brain functional network with highly connected association cortical hubs. *Journal of Neuroscience*, *26*(1), 63–72.

Aghdam, M. A., Sharifi, A., & Pedram, M. M. (2018). Combination of rs-fMRI and sMRI data to discriminate autism spectrum disorders in young children using deep belief network. *Journal of Digital Imaging*, *31*(6), 895–903.

Alexander-Bloch, A., Giedd, J. N., & Bullmore, E. (2013). Imaging structural co-variance between human brain regions. *Nature Reviews Neuroscience*, *14*(5), 322–336.

Alonso Montes, C., Diez, I., Remaki, L., Escudero, I., Mateos, B., Rosseel, Y., & Cortes, J. M. (2015). Lagged and instantaneous dynamical influences related to brain structural connectivity. *Frontiers in Psychology*, *6*, 1024.

Ashburner, J. (2007). A fast diffeomorphic image registration algorithm. *NeuroImage*, *38*(1), 95–113.

Association American Psychiatric. (2013). Diagnostic and statistical manual of mental disorders, 5th edition: DSM-5. *Psychosomatics*, *29*(1), 133–134.

Avlonitou, E., Balatsouras, D. G., Margaritis, E., Giannakopoulos, P., Douniadakis, D., & Tsakanikos, M. (2011). Use of chloral hydrate as a sedative for auditory brainstem response testing in a pediatric population. *International Journal of Pediatric Otorhinolaryngology*, *75*(6), 760–763.

Baron-Cohen, S., Leslie, A. M., & Frith, U. (1985). Does the autistic child have a "theory of mind". *Cognition*, *21*(1), 37–46.

Bassett, D. S., Bullmore, E., Verchinski, B. A., Mattay, V. S., Weinberger, D. R., & Meyer-Lindenberg, A. (2008). Hierarchical organization of human cortical networks in health and schizophrenia. *Journal of Neuroscience*, *28*(37), 9239–9248.

Bassett, D. S., & Bullmore, E. T. (2017). Small-world brain networks revisited. *The Neuroscientist*, *23*(5), 499–516.

Benjamini, Y., & Hochberg, Y. (1995). Controlling the false discovery rate: A practical and powerful approach to multiple testing. *Journal of the Royal Statistical Society: Series B: Methodological*, *57*(1), 289–300.

Bethlehem, R. A., Romero-Garcia, R., Mak, E., Bullmore, E., & Baron-Cohen, S. (2017). Structural covariance networks in children with autism or ADHD. *Cerebral Cortex*, *27*(8), 4267–4276.

Billeci, L., Calderoni, S., Tosetti, M., Catani, M., & Muratori, F. (2012). White matter connectivity in children with autism spectrum disorders: A tract-based spatial statistics study. *BMC Neurology*, *12*(1), 148.

Botev, Z. I., Grotowski, J. F., & Kroese, D. P. (2010). Kernel density estimation via diffusion. *The Annals of Statistics*, *38*(5), 2916–2957.

Bullmore, E., & Sporns, O. (2012). The economy of brain network organization. *Nature Reviews Neuroscience*, *13*(5), 336–349.

Bullmore, E. T., Suckling, J., Overmeyer, S., Rabe-Hesketh, S., Taylor, E., & Brammer, M. J. (1999). Global, voxel, and cluster tests, by theory and permutation, for a difference between two groups of structural MR images of the brain. *IEEE Transactions on Medical Imaging*, *18*(1), 32–42.

Cao, M., He, Y., Dai, Z., Liao, X., Jeon, T., Ouyang, M., & Dong, Q. (2017). Early development of functional network segregation revealed by connectomic analysis of the preterm human brain. *Cerebral Cortex*, *27*(3), 1949–1963.

Cherkassky, V. L., Kana, R. K., Keller, T. A., & Just, M. A. (2006). Functional connectivity in a baseline resting-state network in autism. *Neuroreport*, *17*(16), 1687–1690.

Chung, M., Adluru, N., Dalton, K., Alexander, A., & Davidson, R. (2010). *Characterization of structural connectivity in autism using graph networks with DTI*. Paper presented at the 16th Annual Meeting in Organization for Human Brain Mapping, Barcelona, Spain.

Chung, M. K., Adluru, N., Dalton, K. M., Alexander, A. L., & Davidson, R. J. (2011). *Scalable brain network construction on white matter fibers*. Paper presented at the medical imaging 2011: Image processing.

Cuadra, M. B., Cammoun, L., Butz, T., Cuisenaire, O., & Thiran, J.-P. (2005). Comparison and validation of tissue modelization and statistical classification methods in T1-weighted MR brain images. *IEEE Transactions on Medical Imaging*, *24*(12), 1548–1565.

Damarla, S. R., Keller, T. A., Kana, R. K., Cherkassky, V. L., Williams, D. L., Minshew, N. J., & Just, M. A. (2010). Cortical underconnectivity coupled with preserved visuospatial cognition in autism: Evidence from an fMRI study of an embedded figures task. *Autism Research*, *3*(5), 273–279.

Dennis, E. L., Jahanshad, N., Rudie, J. D., Brown, J. A., Johnson, K., McMahon, K. L., & Wright, M. J. (2011). Altered structural brain connectivity in healthy carriers of the autism risk gene, CNTNAP2. *Brain Connectivity*, *1*(6), 447–459.

Di Martino, A., Kelly, C., Grzadzinski, R., Zuo, X.-N., Mennes, M., Mairena, M. A., & Milham, M. P. (2011). Aberrant striatal functional connectivity in children with autism. *Biological Psychiatry*, *69*(9), 847–856.

Diez, I., Bonifazi, P., Escudero, I., Mateos, B., Muñoz, M. A., Stramaglia, S., & Cortes, J. M. (2015). A novel brain partition highlights the modular skeleton shared by structure and function. *Scientific Reports*, *5*, 10532.

Duan, X., Long, Z., Chen, H., Liang, D., Qiu, L., Huang, X., & Gong, Q. (2014). Functional organization of intrinsic connectivity networks in Chinese-chess experts. *Brain Research*, *1558*, 33–43.

Duan, X., Wang, R., Xiao, J., Li, Y., Huang, X., Guo, X., & Ling, Z. (2020). Subcortical structural covariance in young children with autism spectrum disorder. *Progress in Neuro-Psychopharmacology and Biological Psychiatry*, *99*, 109874.

Eisen, M. B., Spellman, P. T., Brown, P. O., & Botstein, D. (1998). Cluster analysis and display of genome-wide expression patterns. *Proceedings of the National Academy of Sciences*, *95*(25), 14863–14868.

Evans, A. C. (2013). Networks of anatomical covariance. *NeuroImage*, *80*, 489–504.

Fair, D. A., Cohen, A. L., Power, J. D., Dosenbach, N. U., Church, J. A., Miezin, F. M., & Petersen, S. E. (2009). Functional brain networks develop from a "local to distributed" organization. *PLoS Computational Biology*, *5*(5), e1000381.

Fuccillo, M. V. (2016). Striatal circuits as a common node for autism pathophysiology. *Frontiers in Neuroscience*, *10*, 27.

Gao, W., Gilmore, J. H., Giovanello, K. S., Smith, J. K., Shen, D., Zhu, H., & Lin, W. (2011). Temporal and spatial evolution of brain network topology during the first two years of life. *PLoS One*, *6*(9), e25278.

Gong, G., He, Y., Concha, L., Lebel, C., Gross, D. W., Evans, A. C., & Beaulieu, C. (2009). Mapping anatomical connectivity patterns of human cerebral cortex using in vivo diffusion tensor imaging tractography. *Cerebral Cortex*, *19*(3), 524–536.

Gori, I., Giuliano, A., Muratori, F., Saviozzi, I., Oliva, P., Tancredi, R., & Retico, A. (2015). Gray matter alterations in young children with autism spectrum disorders: Comparing morphometry at the voxel and regional level. *Journal of Neuroimaging*, *25*(6), 866–874.

Gotts, S. J., Simmons, W. K., Milbury, L. A., Wallace, G. L., Cox, R. W., & Martin, A. (2012). Fractionation of social brain circuits in autism spectrum disorders. *Brain*, *135*(9), 2711–2725.

Gunaydin, L. A., & Kreitzer, A. C. (2016). Cortico–basal ganglia circuit function in psychiatric disease. *Annual Review of Physiology*, *78*, 327–350.

Guo, X., Duan, X., Chen, H., He, C., Xiao, J., Han, S., & Chen, H. (2020). Altered inter-and intrahemispheric functional connectivity dynamics in autistic children. *Human Brain Mapping*, *41*(2), 419–428.

He, C., Chen, H., Uddin, L. Q., Erramuzpe, A., Bonifazi, P., Guo, X., & Li, L. (2020). Structure–function Connectomics reveals aberrant developmental trajectory occurring at preadolescence in the autistic brain. *Cerebral Cortex*, *30*, 5028–5037.

He, Y., Chen, Z. J., & Evans, A. C. (2007). Small-world anatomical networks in the human brain revealed by cortical thickness from MRI. *Cerebral Cortex*, *17*(10), 2407–2419.

Hilton, C. L., Harper, J. D., Kueker, R. H., Lang, A. R., Abbacchi, A. M., Todorov, A., & LaVesser, P. D. (2010). Sensory responsiveness as a predictor of social severity in children with high functioning autism spectrum disorders. *Journal of Autism and Developmental Disorders*, *40*(8), 937–945.

Horwitz, B., Rumsey, J. M., Grady, C. L., & Rapoport, S. I. (1988). The cerebral metabolic landscape in autism: Intercorrelations of regional glucose utilization. *Archives of Neurology*, *45*(7), 749–755.

Im, W. Y., Ha, J. H., Kim, E. J., Cheon, K.-A., Cho, J., & Song, D.-H. (2018). Impaired white matter integrity and social cognition in high-function autism: Diffusion tensor imaging study. *Psychiatry Investigation*, *15*(3), 292–299.

Jan, M. M., & Aquino, M. F. (2001). The use of choral hydrate in pediatric electroencephalography. *Neurosciences*, *6*(2), 99–102.

Just, M. A., Cherkassky, V. L., Keller, T. A., Kana, R. K., & Minshew, N. J. (2007). Functional and anatomical cortical underconnectivity in autism: Evidence from an FMRI study of an executive function task and corpus callosum morphometry. *Cerebral Cortex*, *17*(4), 951–961.

Just, M. A., Cherkassky, V. L., Keller, T. A., & Minshew, N. J. (2004). Cortical activation and synchronization during sentence comprehension in high-functioning autism: Evidence of underconnectivity. *Brain*, *127*(8), 1811–1821.

Kana, R. K., Libero, L. E., & Moore, M. S. (2011). Disrupted cortical connectivity theory as an explanatory model for autism spectrum disorders. *Physics of Life Reviews*, *8*(4), 410–437.

Kong, X.-Z., Liu, Z., Huang, L., Wang, X., Yang, Z., Zhou, G., & Liu, J. (2015). Mapping individual brain networks using statistical similarity in regional morphology from MRI. *PLoS One*, *10*(11), e0141840.

Kong, X.-Z., Wang, X., Huang, L., Pu, Y., Yang, Z., Dang, X., & Liu, J. (2014). Measuring individual morphological relationship of cortical regions. *Journal of Neuroscience Methods*, *237*, 103–107.

Koshino, H., Carpenter, P. A., Minshew, N. J., Cherkassky, V. L., Keller, T. A., & Just, M. A. (2005). Functional connectivity in an fMRI working memory task in high-functioning autism. *NeuroImage*, *24*(3), 810–821.

Kullback, S., & Leibler, R. A. (1951). On information and sufficiency. *The Annals of Mathematical Statistics*, *22*(1), 79–86.

Lim, H. K., Jung, W. S., & Aizenstein, H. J. (2013). Aberrant topographical organization in gray matter structural network in late life depression: A graph theoretical analysis. *International Psychogeriatrics*, *25*(12), 1929–1940.

Liu, H., Jiang, H., Bi, W., Huang, B., Li, X., Wang, M., & Tao, X. (2019). Abnormal gray matter structural covariance networks in children with bilateral cerebral palsy. *Frontiers in Human Neuroscience*, *13*, 343.

Liu, J., Yao, L., Zhang, W., Xiao, Y., Liu, L., Gao, X., & Gong, Q. (2017). Gray matter abnormalities in pediatric autism spectrum disorder: A meta-analysis with signed differential mapping. *European Child & Adolescent Psychiatry*, *26*(8), 933–945.

Lord, C., Risi, S., Lambrecht, L., Cook, E. H., Leventhal, B. L., DiLavore, P. C., & Rutter, M. (2000). The autism diagnostic observation schedule—Generic: A standard measure of social and communication deficits associated with the spectrum of autism. *Journal of Autism and Developmental Disorders*, *30*(3), 205–223.

Matsuzaki, J., Kagitani-Shimono, K., Goto, T., Sanefuji, W., Yamamoto, T., Sakai, S., & Yorifuji, S. (2012). Differential responses of primary auditory cortex in autistic spectrum disorder with auditory hypersensitivity. *Neuroreport*, *23*(2), 113–118.

Maximo, J. O., & Kana, R. K. (2019). Aberrant "deep connectivity" in autism: A cortico–subcortical functional connectivity magnetic resonance imaging study. *Autism Research*, *12*(3), 384–400.

McAlonan, G. M., Cheung, V., Cheung, C., Suckling, J., Lam, G. Y., Tai, K., & Chua, S. E. (2005). Mapping the brain in autism. A voxel-based MRI study of volumetric differences and intercorrelations in autism. *Brain*, *128*(2), 268–276.

Murias, M., Webb, S. J., Greenson, J., & Dawson, G. (2007). Resting state cortical connectivity reflected in EEG coherence in individuals with autism. *Biological Psychiatry*, *62*(3), 270–273.

Noriuchi, M., Kikuchi, Y., Yoshiura, T., Kira, R., Shigeto, H., Hara, T., & Kamio, Y. (2010). Altered white matter fractional anisotropy and social impairment in children with autism spectrum disorder. *Brain Research*, *1362*, 141–149.

Olivier, T. W., Mahone, E. M., & Jacobson, L. A. (2018). Wechsler intelligence scale for children. *Canadian Journal of School Psychology*, *19* (Suppl 1), 221–234.

Park, H.-J., & Friston, K. (2013). Structural and functional brain networks: From connections to cognition. *Science*, *342*(6158), 1238411.

Power, J. D., Fair, D. A., Schlaggar, B. L., & Petersen, S. E. (2010). The development of human functional brain networks. *Neuron*, *67*(5), 735–748.

Raj, A., Mueller, S. G., Young, K., Laxer, K. D., & Weiner, M. (2010). Network-level analysis of cortical thickness of the epileptic brain. *NeuroImage*, *52*(4), 1302–1313.

Rasero, J., Jimenez-Marin, A., Diez, I., Hasan, M. T., & Cortes, J. M. (2020). Genes involved in cholesterol cascades are linked to brain connectivity in one third of autistic patients. *bioRxiv*.

Rosenberg, M. D., Finn, E. S., Scheinost, D., Papademetris, X., Shen, X., Constable, R. T., & Chun, M. M. (2016). A neuromarker of sustained attention from whole-brain functional connectivity. *Nature Neuroscience*, *19*(1), 165–171.

Rumm, P., Takao, R., Fox, D., & Atkinson, S. (1990). Efficacy of sedation of children with chloral hydrate. *Southern Medical Journal*, *83*(9), 1040–1043.

Saggar, M., Hosseini, S. H., Bruno, J. L., Quintin, E.-M., Raman, M. M., Kesler, S. R., & Reiss, A. L. (2015). Estimating individual contribution from group-based structural correlation networks. *NeuroImage*, *120*, 274–284.

Schipul, S. E., Keller, T. A., & Just, M. A. (2011). Inter-regional brain communication and its disturbance in autism. *Frontiers in Systems Neuroscience*, *5*, 10.

Shen, X., Finn, E. S., Scheinost, D., Rosenberg, M. D., Chun, M. M., Papademetris, X., & Constable, R. T. (2017). Using connectome-based predictive modeling to predict individual behavior from brain connectivity. *Nature Protocols*, *12*(3), 506–518.

Sisson, D. F., & Siegel, J. (1989). Chloral hydrate anesthesia: EEG power spectrum analysis and effects on VEPs in the rat. *Neurotoxicology and Teratology*, *11*(1), 51–56.

Sparks, B., Friedman, S., Shaw, D., Aylward, E. H., Echelard, D., Artru, A., & Dawson, G. (2002). Brain structural abnormalities in young children with autism spectrum disorder. *Neurology*, *59*(2), 184–192.

Supekar, K., Musen, M., & Menon, V. (2009). Development of large-scale functional brain networks in children. *PLoS Biology*, *7*(7), e1000157.

Tijms, B. M., Seriès, P., Willshaw, D. J., & Lawrie, S. M. (2012). Similarity-based extraction of individual networks from gray matter MRI scans. *Cerebral Cortex*, *22*(7), 1530–1541.

Tohka, J., Zijdenbos, A., & Evans, A. (2004). Fast and robust parameter estimation for statistical partial volume models in brain MRI. *NeuroImage*, *23*(1), 84–97.

Tzourio-Mazoyer, N., Landeau, B., Papathanassiou, D., Crivello, F., Etard, O., Delcroix, N., & Joliot, M. (2002). Automated anatomical labeling of activations in SPM using a macroscopic anatomical parcellation of the MNI MRI single-subject brain. *NeuroImage*, *15*(1), 273–289.

Van Den Heuvel, M. P., Kersbergen, K. J., De Reus, M. A., Keunen, K., Kahn, R. S., Groenendaal, F., & Benders, M. J. (2015). The neonatal connectome during preterm brain development. *Cerebral Cortex*, *25*(9), 3000–3013.

Wang, H., Jin, X., Zhang, Y., & Wang, J. (2016). Single-subject morphological brain networks: Connectivity mapping, topological characterization and test–retest reliability. *Brain and Behavior: A Cognitive Neuroscience Perspective*, *6*(4), e00448.

Wang, J., Fu, K., Chen, L., Duan, X., Guo, X., Chen, H., & Chen, H. (2017). Increased gray matter volume and resting-state functional connectivity in somatosensory cortex and their relationship with autistic symptoms in young boys with autism spectrum disorder. *Frontiers in Physiology*, *8*, 588.

Wang, J., Wang, X., Xia, M., Liao, X., Evans, A., & He, Y. (2015). GRETNA: A graph theoretical network analysis toolbox for imaging connectomics. *Frontiers in Human Neuroscience*, *9*, 386.

Wang, X.-H., Jiao, Y., & Li, L. (2020). A unified framework for mapping individual interregional high-order morphological connectivity based on regional cortical features from anatomical MRI. *Magnetic Resonance Imaging*, *66*, 232–239.

Watts, D. J., & Strogatz, S. H. (1998). Collective dynamics of 'small-world'networks. *Nature*, *393*(6684), 440–442.

Wechsler, D. (1949). Wechsler intelligence scale for children.

Yerys, B. E., Herrington, J. D., Satterthwaite, T. D., Guy, L., Schultz, R. T., & Bassett, D. S. (2017). Globally weaker and topologically different: Resting-state connectivity in youth with autism. *Molecular Autism*, *8*(1), 1–11.

Yun, J.-Y., Boedhoe, P. S., Vriend, C., Jahanshad, N., Abe, Y., Ameis, S. H., & Benedetti, F. (2020). Brain structural covariance networks in obsessive-compulsive disorder: A graph analysis from the ENIGMA consortium. *Brain*, *143*(2), 684–700.

Zalesky, A., Fornito, A., & Bullmore, E. T. (2010). Network-based statistic: Identifying differences in brain networks. *NeuroImage*, *53*(4), 1197–1207.

Zhang, J., Wang, J., Wu, Q., Kuang, W., Huang, X., He, Y., & Gong, Q. (2011). Disrupted brain connectivity networks in drug-naive, first-episode major depressive disorder. *Biological Psychiatry*, *70*(4), 334–342.

Zhang, Z., Liao, W., Chen, H., Mantini, D., Ding, J.-R., Xu, Q., & Jiao, Q. (2011). Altered functional–structural coupling of large-scale brain networks in idiopathic generalized epilepsy. *Brain*, *134*(10), 2912–2928.

Zhao, W., Guo, S., Linli, Z., Yang, A. C., Lin, C.-P., & Tsai, S.-J. (2020). Functional, anatomical, and morphological networks highlight the role of basal ganglia–thalamus–cortex circuits in schizophrenia. *Schizophrenia Bulletin*, *46*(2), 422–431.

Zhou, L., Wang, Y., Li, Y., Yap, P.-T., Shen, D., & Initiative, A. s. D. N. (2011). Hierarchical anatomical brain networks for MCI prediction: Revisiting volumetric measures. *PLoS One*, *6*(7), e21935.

Zilbovicius, M., Garreau, B., Samson, Y., Remy, P., Barthelemy, C., Syrota, A., & Lelord, G. (1995). Delayed maturation of the frontal cortex in childhood autism. *The American Journal of Psychiatry*, *152*(2), 248–252.

Zou, T.-X., She, L., Zhan, C., Gao, Y.-Q., & Chen, H.-J. (2018). Altered topological properties of gray matter structural covariance networks in minimal hepatic encephalopathy. *Frontiers in Neuroanatomy*, *12*, 101.

SUPPORTING INFORMATION

Additional supporting information may be found online in the Supporting Information section at the end of this article.

How to cite this article: He C, Cortes JM, Kang X, et al. Individual-based morphological brain network organization and its association with autistic symptoms in young children with autism spectrum disorder. *Hum Brain Mapp*. 2021;1–13. https://doi.org/10.1002/hbm.25434